Luminescent characteristics of Eu^{2+}/Li^{+} doped $(La\text{-}Al)_2O_3$ phosphors and PMMA films activated with them

L. Mariscal-Becerra[a,e,*], S. Carmona-Téllez[b], G. Alarcón-Flores[b], J.U. Balderas-Aguilar[c], R. Vázquez-Arreguín[d], H. Murrieta[a], and C. Falcony[d]

[a]*Instituto de Física de la Universidad Nacional Autónoma de México, Circuito de la Investigación Científica, Ciudad Universitaria Coyoacán, 04510, México CDMX.*

[b]*Instituto Politécnico Nacional, Centro de Investigación en Ciencia Aplicada y Tecnología Avanzada, Unidad Legaria, Calzada Legaria 694, Irrigación, Miguel Hidalgo, 11500, México, CDMX.*

[c]*Centro de Investigación y de Estudios Avanzados del IPN, Programa de Doctorado en Nanociencias y Nanotecnología, Av. Instituto Politécnico Nacional 2508 San Pedro Zacatenco, Gustavo A. Madero, 07360, México CDMX.*

[d]*Instituto Politécnico Nacional, Escuela Superior de Cómputo, Av. Juan de Dios Bátiz esq. Av. Miguel Othón de Mendizábal, Lindavista, Gustavo A. Madero, México, 07738, CDMX.*

[e]*Departamento de Física del Centro de Investigación y de Estudios Avanzados del IPN. Av. Instituto Politécnico Nacional 2508 San Pedro Zacatenco, Gustavo A. Madero, 07360 México CDMX.*

Received 14 March 2018; accepted 16 May 2018

The effect of Li co-doping on the blue luminescence of Eu^{2+} doped $(La\text{-}Al)_2O_3$ phosphors and its incorporation into poly (methyl methacrylate) PMMA films are reported. The phosphors were synthesized by a simple two-step process in which the $(La\text{-}Al)_2O_3$ powders were obtained by an evaporation method, and the subsequent co-doping with Li^{+} and Eu^{2+} were made through a solid state reaction in a reductive atmosphere at 1250°C. The incorporation of those phosphors into PMMA matrix and the synthesis of films with thicknesses between 6 and 12 μm was made by drop-casting. The characteristic blue broad band emission centered at 440 nm associated with the $4f^6 5d^1 \rightarrow 4F^7$ transition of Eu^{2+} ions (CIE coordinates 0.6731, 0.3343) was observed when these powders were excited with 297 nm light. These luminescence intensity was enhanced when Li^{+} was incorporated as co-dopant up to 320% with respect to those phosphors without Lithium. The luminescent characteristics of these phosphors were preserved when they were embedded into the PMMA films.

Keywords: Eu^{2+} blue emission; lithium effect; PMMA composite films.

PACS: 42; 42.70.-a; 81; 81.10.St

1. Introduction

The development of new phosphors, which can be activated in the UV region (300-420 nm), has received especial attention in recent years due to the need to increase the efficiency of white light emission in solid state lighting (SSL) devices. White light emitting diodes (WLEDs) are regarded as the next generation lighting source due to their long lifetime, environmental friendliness, and high efficiency, compared with conventional incandescent and fluorescence lamps. The main strategy to obtain WLEDs is known as phosphor converted-LEDs (pc-LEDs), *i.e.* the combination of blue or near-ultraviolet (n-UV) LEDs with one or more phosphors. The most commercial approach is a blue InGaN based LED with a $Y_3Al_5O_{12}$:Ce^{3+} (YAG: Ce) phosphor [1]. However, this approach has problems with its low color rendering characteristic. Another approach to get white light is the combination of a near UV LED (300-420 nm) with tricolor phosphors (red, green and blue).Thornton (1971) showed that mixing of discrete emission bands with peak wavelengths near 450, 540 and 610 nm resulted in a high-quality white light source [2]; however, high intensity blue emission is hard to be achieved using rare earths such as cerium or thulium, while green and red emissions are relatively easily generated through the use of Tb^{3+} and Eu^{3+} ions respectively [3-5]. In order to solve this problem, some reports have proposed Eu^{2+} ions as dopant in different kind of matrices [6,7]. The lanthanides have similar electronic configuration among them, because they have partially filled the 4f shell and generally adopt 3+ (RE^{3+}) ionic state. One characteristic of this ions is that their light emission is almost the same regardless of the host material in which they are immersed, this is because their 4f electrons are shielded by $5s^2$ and $5p^6$ electrons; therefore the host lattice has little influence in the optical transitions that occur in these ions. However, in RE^{2+} ions, the luminescence occurs through energy transitions between the $4f^7$ and $4f^6 5d^1$ electronic energy levels. In this case the exact transition energy values involved depend on the crystalline field that surrounds the ion in the host lattice [8], since in this case no shielding occurs for the electrons in the 5d excited state. Also, since these transitions are electric-dipole allowed, they are highly efficient. Concerning the host matrix for these ions, there is a wide variety of materials such as silicates, aluminates, sulfides, oxides, phosphates, borates glasses, etc. [3-5,9-13] which have been doped with RE. These compounds, in general, are synthetized by different techniques such as spray pyrolysis [14], solvent evaporation

[3-5], mechanochemical synthesis [15], soft chemical synthesis [16], solid state reaction at high temperatures in an inert atmosphere [6], vibrating milled solid-state reaction [17], coprecipitation method [18], etc. In the case of Eu^{2+} ions, the use of $LaAlO_3$ has been investigated in consideration to the radii fit (Eu^{2+} (0.14 nm) or Eu^{3+} (0.13 nm) for La^{3+} (0.15 nm) [19].

Complementary to the synthesis of phosphors, there is a need to handle these materials in the form of coatings with properties like mechanical flexibility, environment friendly and low manufacturing cost. Polymer films offer all these properties and some of them can be synthesized as composites with the above mentioned phosphors to have luminescent properties through RE doping. These films have been sensitized by many techniques such as: spin-coating, sol-gel, spray pyrolysis and MAPLE (matrix assisted pulsed laser evaporation) among others. According to some previous reports, many techniques have synthesized polymer films, such as spin coating, sol-gel and spray pyrolysis among others. The polymethylmethacrylate (PMMA) is thermoplastic which presents good chemical and thermal stabilities, flexibility and very high transparency (92 up to 99% T, between 220 to 1500 nm); for these reasons, PMMA is an excellent candidate to be used as a coating in solar cell devices [20].

In this paper the luminescent, structural and morphological characteristics of Li^+, and Eu^{2+} doped $(La\text{-}Al)_2O_3$ phosphors and its subsequent incorporation into PMMA films fabricated by the drop cast technique are reported. These PMMA films have potential applications in short-wavelength optoelectronic devices, such as luminescent materials, transparent light emitters, thin-film gas sensors, and solar cell enhancers.

2. Experimental section

Synthesis of phosphors

The Li^+, and Eu^{2+} doped $(La\text{-}Al)_2O_3$ phosphors were obtained by simple evaporation technique and solid state reaction in an reductive atmosphere, using a constant amount of lanthanum chloride (2 at.%); appropriate amounts of the other precursors, in the form of chlorides, were dissolved in 5 ml of deionized water (18 MΩ-cm^{-1}) and then it was heated at 200°C to obtain La-Al-O powder; then, an atmospheric annealing for 2 hr at 700°C was given to this powders to obtain the properly synthesized oxide matrix. The Eu^{2+} luminescence activator was added through a solid state reaction process with these powders and $EuCl_2$ (1, 3, 5, and 7 at. %) at 1250°C for 2 hrs. In a reductive atmosphere (using forming gas which is composed by 20% hydrogen and 80% nitrogen); finally the phosphors which showed the best luminescence intensity, Eu^{2+} (5at%) as described below, were co-doped with lithium (0.5, 1.0, 1.5, 3.0, 4.5 and 6.0 at.%), also through solid state reaction with LiCl in a reductive atmosphere at 1250°C, (in this case lithium and europium raw materials are added at the same time, before the heat treatment at 1250°C), the phosphor with 4.5% Li presented the most intense luminescence emission.

Synthesis of PMMA

20 ml of methyl methacrylate monomer (MMA) was dissolved in 80 ml of toluene and 0.048 g of benzoyl peroxide (BPO) was then added. Polymerization reaction was carried out in a 500 ml three-neck flask connected to a high purity nitrogen inlet, a condenser and a thermometer. The solution was heated at 70°C under magnetic stirring for 10 hours. The reaction mixture was then precipitated in methanol and the resulting PMMA polymer was dried under vacuum at 60°C for 24 h.

Surface functionalization of the $(La\text{-}Al)_2O_3$ Eu^{2+} phosphors

In order to disperse the phosphor powders in the PMMA matrix, trioctylphosphine oxide (TOPO) was used to functionalize the phosphors. In a typical experiment 0.1 g of the phosphors were dissolved in 10 ml chloroform ($CHCl_3$) by magnetic stirring for 1 h followed by ultrasonic stirring for 1h. 0.02 g of TOPO were then added to the main solution under vigorous magnetic stirring and the resulting colloidal suspension was ultrasonically stirred for 4 h more. The resulting material was centrifuged, rinsed with $CHCl_3$ and dried in vacuum overnight.

Synthesis of the composite $(La\text{-}Al)_2O_3$ Eu^{2+}/PMMA films

PMMA was dissolved in $CHCl_3$ at 2% (w/v) at room temperature. Then a controlled amount of functionalized (lanthanum-aluminum-Eu^{2+}) particles (50 wt% respect to PMMA) was added to the solution under vigorous magnetic stirring for 2 h. The solution was drop-casted on corning glass substrates and slowly dried at room temperature for 24 h, the films were then fully dried in an oven at 60°C for 2 h. Four films thicknesses were obtained by casting four different quantities of solution (1, 1.2, 1.3 and 1.4 ml).

Characterization Equipment

Luminescence spectra were obtained with an Edinburgh Inst. Spectrofluorometer, Mod. 980S. The chemical composition was measured using energy dispersive spectroscopy (EDS) with a Leica Cambridge model Stereoscan Electron Microscope equipped with a detector 440 X-ray beryllium window. CL measurements were performed in a stainless steel vacuum chamber with a cold cathode electron gun (Luminoscope, model ELM-2 MCA, RELION Co.). In this case, the emitted light was collected by an optical fiber and fed into a SPEX Fluoro-Max-P spectrophotometer; all measurements were carried out at room temperature. The crystalline structure was analyzed by X-ray diffraction (XRD) using a Siemens D5000 diffractometer with 1.540 Å (Cu Kα) operating at 30 keV. SEM images were obtained on a Scanning Electron Microscope JEOL using an accelerating voltage of 20

kV and higher X5000 in Al_2O_3 powders. XPS analysis was performed with Thermo Scientific K analysis surface, spot size 400 μm and emission from Aluminum K-α, the resolution to the surface with 1 eV and extensive analysis step size of 0.1 eV. Thickness measurements were obtained on a KLA Tecnor Mod. D-600 Profiler. Optical transmittance spectra were obtained with a Perkin Elmer Lambda 25 spectrophotometer in a wavelength range of 200 to 1100 nm. IR spectroscopy measurements were made in a 6700 FT-IR NICOLET and spectrum Raman with a WITec combined Confocal Raman Imaging and Atomic Force Microscope System, highest sensitivity for 633 nm excitation wavelength.

3. Results & Discussion

Phosphors

Figure 1 shows XRD diffractograms for $(La\text{-}Al)_2\ O_3$, $(La\text{-}Al)_2O_3$:Eu^{2+}/(5 at. %) and $(La\text{-}Al)_2O_3$:Eu^{2+}(5at.%)/Li^{+} (4.5 at. %) host matrix and phosphors, and the reported diffraction patterns for $La_{(0.827)}Al_{(11.9)}O_{(19.09)}$ (No: 01-077-0311, CSD: 38371(ICSD) and for $LaAlO_3$ perovskite (No: 01-073-3684, CSD: 170772(ICSD). The undoped $(La\text{-}Al)_2O_3$ diffractogram indicates that it is mostly amorphous material, although two broad reflexes at 45° and 67° might point to the initial stages of the (206) and (220) reflexes associated with the $La_{(0.827)}\ Al_{(11.9)}\ O_{(19.09)}$ phase. Samples

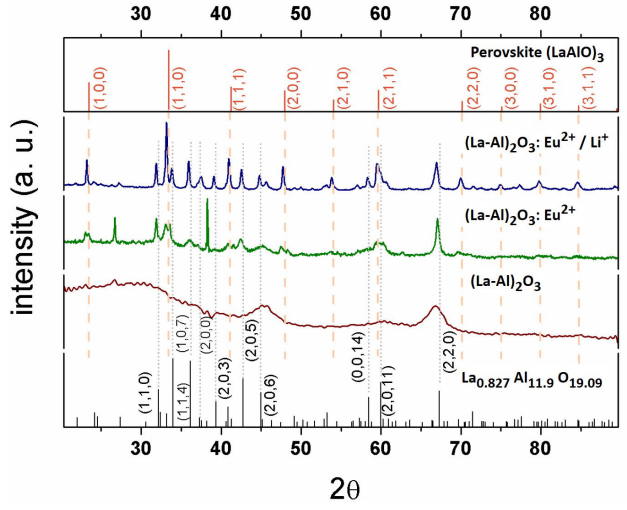

FIGURE 1. XRD measurements from $(La\text{-}Al)_2O_3$, $(La\text{-}Al)_2O_3$:Eu^{2+}/(5 at. %) and $(La\text{-}Al)_2O_3$:Eu^{2+}(5at.%)/Li^{+}(4.5 at. %) phosphors.

doped with Eu^{2+} and Eu^{2+} plus Li^{+}, on the other hand, present diffraction reflexes that establish the polycrystalline nature of these phosphors. From these data is clear that Eu^{2+} and Eu^{2+}/Li^{+} doping propitiate the formation of a polycrystalline material mostly identified with either the $La_{(0.827)}Al_{(11.9)}O_{(19.09)}$ phase and the $LaAlO_3$ phase, in particular, the phosphors with Eu^{2+} doping alone have an estimated content of 94 and 6% determined by weight ratio for each phase, respectively with crystallite size of approximately 1nm estimated by Halder-Wagner method. The co-doping with Li promotes the formation of larger crystallites (about 11 nm) with 92 and 8% composition of the same crystalline phases. It is important to note that the desired phase was the $La_{(0.827)}Al_{(11.9)}O_{(19.09)}$ one; however, as it was mentioned before, the synthesis process needs two steps in order to incorporate the Eu^{2+} ions; and the second step is a heat treatment at 1250°C which leads to a rearrangement of the crystalline structure, reaching a partial presence of the perovskite phase, which is richer in lanthanum than the $La_{(0.827)}Al_{(11.9)}O_{(19.09)}$ phase. This behavior is reflected in the EDS results, where a slight decrease in the aluminum content and a proportional increase of the lanthanum was observed. Table I lists the EDS measurements for the undoped, Eu^{2+} (5 at. %) and Eu^{2+} plus Li^{+} (4.5 at. %) phosphors; as it could be observed, the desired $La_{(0.827)}Al_{(11.9)}O_{(19.09)}$ phase has 60% of oxygen, 37.4 of aluminum and just 2.6 at. % of lanthanum; however, the achieved composition in synthesized phosphors shows a slight decrease in the aluminum content and a proportional increase of the lanthanum content, as explained above. Since EDS technique is not capable of measuring the content of Li, the composition has been determined only for the rest of the components, all samples presented a stoichiometry close to $(La\text{-}Al)_2O_3$, within the EDS technique precision. The Eu^{2+} doped samples present a 0.7 at % content of Eu, which most likely, is incorporated in substitution of La sites because their radii similitude, this amount of Eu^{2+} is low in comparison with the starting dopant content in the source material, this behavior is common in synthesis techniques which operate under atmospheric pressure and gas fluxes (as in this case) [21,22] and has been explained for similar materials considering that the host materials have a saturation limit in their capacity of dopants acceptance, and the un-reacted precursors are eliminated through volatile residues that are clear out from the reaction chamber.

TABLE I. EDS measurements for $(La\text{-}Al)_2O_3$, $(La\text{-}Al)_2O_3$: Eu^{2+} (5 at. %) and $(La\text{-}Al)_2O_3$: Eu^{2+} (5at. %) / Li^{+} (4.5 at. %) phosphors.

$(LaAl)_2O_3$		$(LaAl)_2O_3$:Eu^{2+}(5 at. %)		$(LaAl)_2O_3$:Eu^{2+}(5 at. %)/ Li^{+} (4.5 at. %)	
Element	atomic %	Element	atomic %	Element	atomic %
O	63.8±3	O	62.3±2	O	60.6±3.4
Al	32.2±2	Al	33.5±2	Al	33.9±1.3
La	4.0±0.6	La	3.5±0.6	La	4.8±0.8
		Eu	0.7±0.1	Eu	0.7±0.1

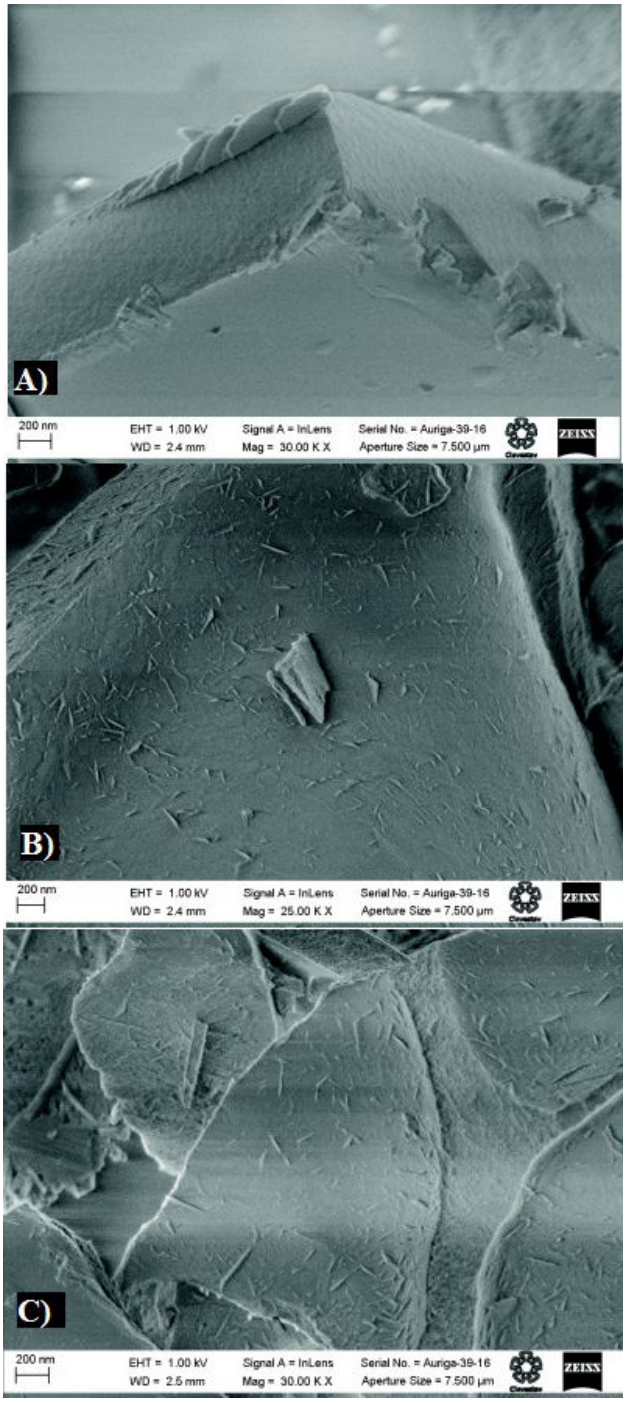

FIGURE 2. SEM images from, A.- (La-Al)$_2$O$_3$, B.- (La-Al)$_2$ O$_3$:Eu^{2+}/(5 at. %) and C.- (La-Al)$_2$O $_3$:Eu^{2+}(5at.%)/Li^{+}(4.5 at. %) phosphors.

Figure 2 shows SEM images for undoped, europium and europium/lithium doped phosphors, these phosphors were mechanically grinded before the annealing processes, therefore they present particles with sharp edges characteristic of this type of grinding process. The Fig. 2a shows a micrograph for undoped powder, it is possible to observe that the particles have low porosity and a smooth surface. In the case of Eu^{2+} (5 at. %) doped phosphors (Fig. 2b), the particles present a needle like texture on their surface. This type of texturing is accentuated for the Eu2+(5at.%)/Li+(4.5 at. %) phosphors, as it is appreciated in Fig. 2c. Considering the X-ray results presented above, it is possible that this texturing is linked with formation of a poly-crystalline structure triggered by the addition of the dopants.

Figure 3a-c shows the normalized XPS results for O1s, Al2p and La3d corresponding to (La-Al)$_2$O$_3$, (La-Al)$_2$O$_3$:Eu^{2+}(5at.%) and (La-Al)$_2$O$_3$:Eu^{2+}(5at.%) / Li^{+}(4.5 at. %) phosphors, Fig. 3d show the binding energy for Li in the last case. Binding energy values were calibrated against the hydrocarbon C 1s line (284.6 eV), present because of contamination by hydrocarbons either from ambient air or from residual gases in the vacuum chamber and were found to be at 531.18, 74.28, and 835.58/838.78 eV for O1s [23], Al2p [24] and La3d$_{5/2}$/3d$_{3/2}$ respectively [25]. The binding energies for Li1s in the case of (La-Al)$_2$O$_3$:Eu^{2+}(5at.%)/Li^{+}(4.5 at. %) phosphor (Fig. 3D), present two peaks, at 51.3 and 54.35 eV. It has been reported previously that the peak close to 54.35 eV corresponds to Li2O while the peak observed close to 51.3 eV is attributed to Li metal [26-28]. Binding energies for Eu^{2+} 3d$_{3/2}$ and Eu^{3+} 3d$_{5/2}$ (not shown) were observed at 1153.8 and 1134.4 eV [29]; a low displacement of the binding energy is observable when the phosphors are doped with lithium (this displacement does not occur in those phosphors without lithium), this shift could be due to oxygen, aluminum and lanthanum having been bound with Li forming species such as Li-O, Li-Al and Li-La. According to the literature [30] when this kind of displacements appears, it is a signal of the formation of different kind of bonds, in the case of the oxygen (Fig. 3a), the species that could be appearing due to the presence of lithium are LiO and Li$_2$O. Although the formation of species between oxygen and Li are so evident it is also possible to observe a low displacement in the case of aluminum (Fig. 3b), thus, it is possible that species such as LiAl and LiAlO may also be generated. Since in the case of lanthanum (Fig. 3c) the shift in energy induced by the incorporation of Li is small, it is possible that the formation of other species is not evident, thus lithium seems to be preferably bound to oxygen (Fig 3a).

The luminescence excitation and emission spectra for the (La-Al)$_2$O$_3$/Eu^{2+} (5 at. %) and (La-Al)$_2$O$_3$):Li^{+} /Eu^{2+}/(5at.%)/Li+(4.5 at. %) phosphors are displayed in Fig. 4. The excitation spectra for both phosphors present two peaks at 273 and 305 nm corresponding to the allowed transitions ^{4}F$_7$ (^{8}S$_{2/7}$)-4f^{6}5d of the ion Eu^{2+} [31], while the emission spectrum (using 297 nm as excitation wavelength) has the characteristic broad emission peak centered at 444 nm (blue light emission, CIE coordinates 0.6731, 0.3343) associated with the electric-dipole allowed 4f$_6$5d$_1$(^{8}S$_{7/2}$) to 4f^7 transition, of the Eu^{2+} ion [32]. There are also, two low peaks at 595 and 614 nm related to the transitions ^{5}D$_0$ to ^{7}F$_1$ and ^{7}F$_2$ respectively from Eu^{3+} ion. The presence of these peaks is a hint that a small amount of the europium undergoes an oxidation process from the 2+ state to the 3+ state, even though the annealing process was carried under a reductive

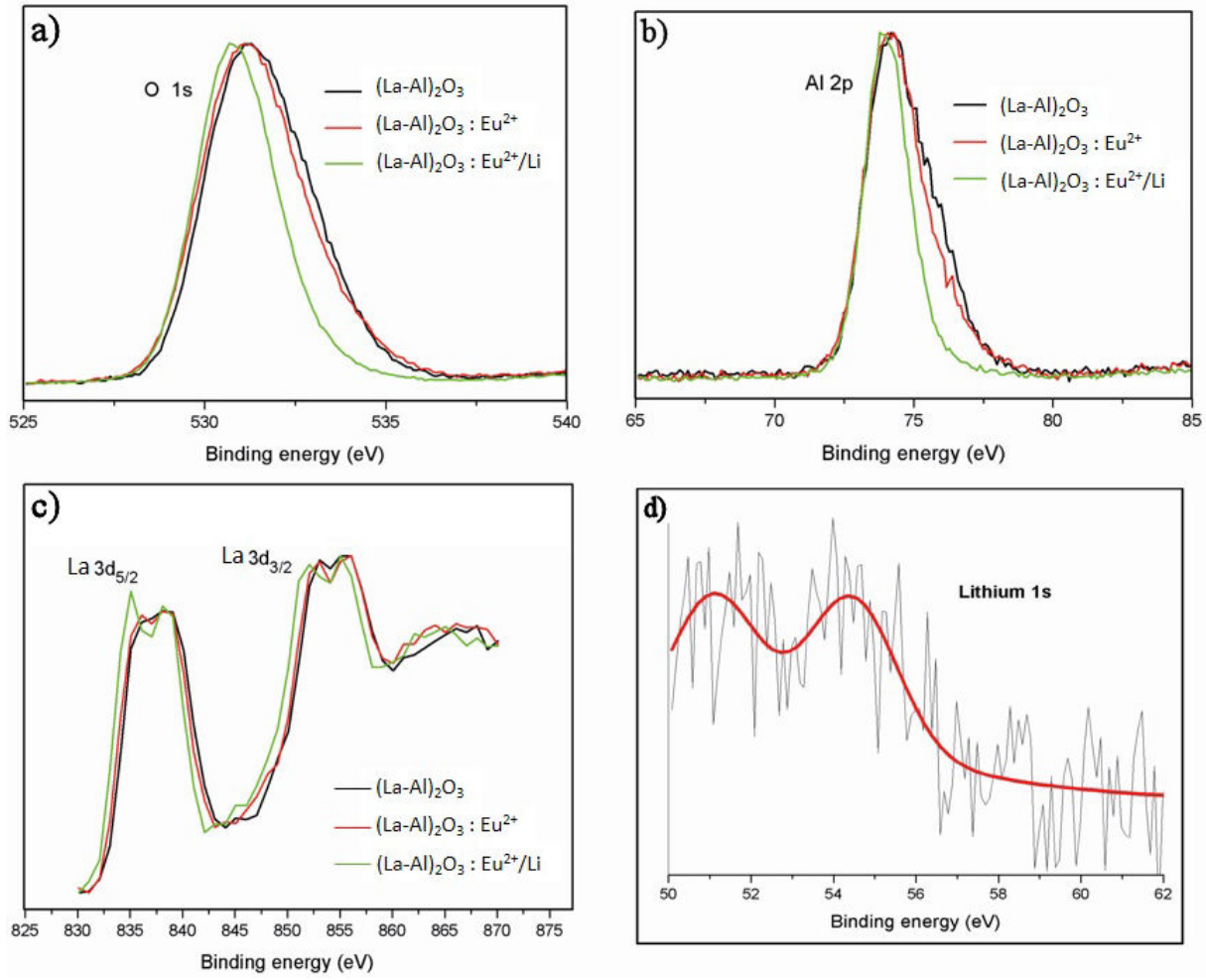

FIGURE 3. XPS measurements, (3A) binding energy O1s, (3B) binding energy Al2p, (3C) binding energy $3d_{5/2}$ and $3d_{3/2}$ of lanthanum and (3D) binding energy of Lithium 1s.

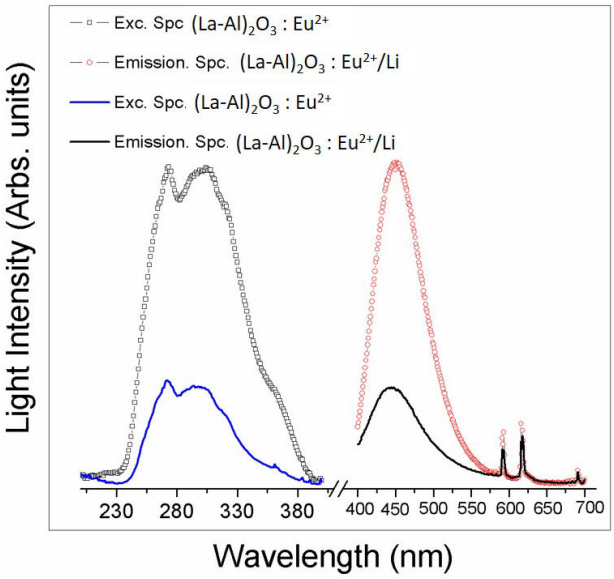

FIGURE 4. Excitation and emission spectra from $(La\text{-}Al)_2O_3$, $(La\text{-}Al)_2O_3$:Eu^{2+}/(5 at. %) and $(La\text{-}Al)_2O_3$:Eu^{2+}(5at.%)/Li^{+}(4.5 at. %) phosphors.

ambient. The main difference between the spectra for the two phosphors is an enhancement in the emission intensity due to the incorporation of lithium ions of about 320%. The role that Li co-doping plays in this luminescent enhancement is not well understood at present, but there are several effects that could add to create the enhancement observed, such as the increment of the crystallinity of the phosphors with the incorporation of Li as described above. Also, the presence of lithium ions create oxygen vacancies, which could work as a required sensitizer needed to create an energy transfer from the host material to the rare earth ions (Eu^{2+} in this case), a luminescence enhancement is the result of this mixing of states in the energy transfer [33,34].

The behavior of the luminescence intensity at the 444 nm peak for phosphors doped with 1, 3, 5 and 7 at. % of Eu^{2+} is shown in Fig. 5 (black dash line) where the peak intensity is plotted as a function of Eu^{2+} concentration. The maximum emission intensity corresponds to phosphors doped with 5 at %, quenching at higher concentrations is probably due the closeness between the Eu^{2+} ions favoring non-radiative processes and a notable decrease of light emission.

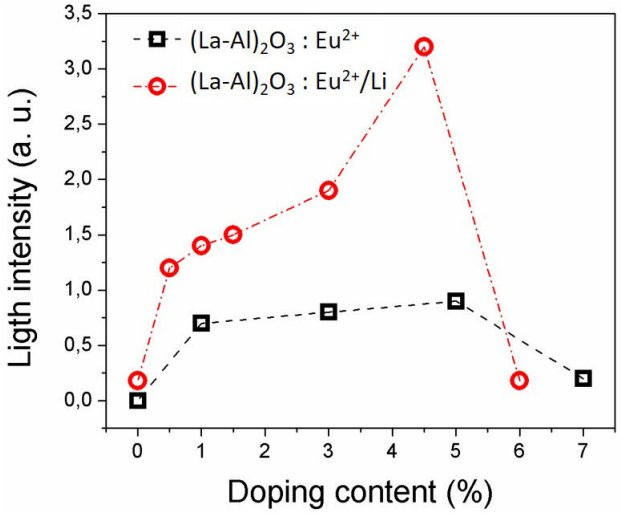

FIGURE 5. Light emission as a function of Eu^{2+} and Li^{+} concentration in (La-Al)$_2O_3$:Eu^{2+} (5 at. %) [black dash line] and (La-Al)$_2O_3$:Eu^{2+} (5at. %)/Li^{+} (4.5 at. %) [Red dash dot line] doped phosphors.

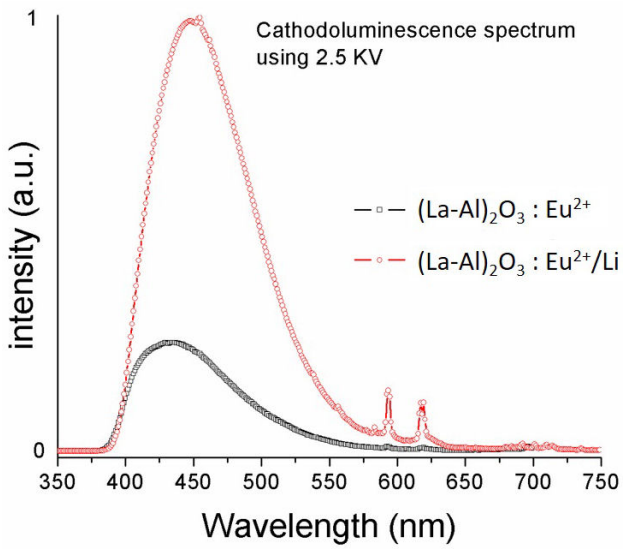

FIGURE 6. CL emission spectrum of (La-Al)$_2O_3$: Eu^{2+} (5 at. %) and (La-Al)$_2O_3$:Eu^{2+}(5at.%)/Li^{+} (4.5 at. %) phosphors.

(La-Al)$_2O_3$:Eu^{2+} (5 at. %) phosphors were co-doped with lithium using the next concentrations: 0.5, 1, 1.5, 3, 4.5 and 6 at. %; Fig. 5 (red dash dot line) shows a maximum luminescence emission at 4.5 at. %, at higher Li^{+} concentrations a quenching phenomenon is also present. The role of lithium doping on (La-Al)$_2O_3$: Eu^{2+} could be to provide an electron that can move within the Eu^{2+}4f orbitals leading to an increase of the luminescent intensity by acting as a charge-balancer, therefore playing the role of a sensitizer. The abrupt quenching of the luminescence intensity for Li content above 4.5 at.% could be due to an abrupt saturation of the level 4f by the lithium content, the excess Li then propitiate the creation of non-radiative alternative ways to dissipate the absorbed energy. As in the case of no-lithium samples, an emission related to Eu^{3+} is also present, but the enhancement of the luminescence, in this case, is much lower than the one observed in the 444 nm peak. The lithium doped phosphors exhibit a measured quantum yield efficiency close 67%, while non-lithium doped phosphors have quantum yield efficiency around 34%, when excited with a 297 nm light [35]. Therefore, the effect of lithium is to enhance the intensity of light emission as well as the quantum yield efficiency.

Frequency domain fluorescence decay measurements (not shown) on (La-Al)$_2O_3$:Eu^{2+}(5at.%)/Li^{+}(4.5 at. %) phosphor, with an excitation wavelength of 297 nm and luminescence wavelength of 440 nm were fitted by a double exponential decay model with $\tau_1 = 592$ ns, $f_1 = 0.9819$ and $\tau_2 = 29$ ns, $f_2 = 0.0181$; and a $\chi^2 = 1.185$. These values are comparable to previously reported values for Eu^{2+} in another host material [36-38], it is known that the d-f transition of Eu^{2+} is parity and spin allowed with a lifetime on the order of sub-microseconds [39,40].

Figure 6 shows the cathode-luminescence (CL) spectra for (La-Al)$_2O_3$:Eu^{2+}(5at.%) and (La-Al)$_2O_3$: Eu^{2+} (5at.%) /Li^{+} (4.5 at. %) phosphors: CL measurements were performed with an anode voltage and beam current, kept constant during the measurement, at 2.5 kV and 1.0 μA respectively. The CL spectra are similar to those observed with the photoluminescence, dominated by the blue emission peak at 444 nm (transition allowed $4f^6 5d^1 \rightarrow 4f^7$ of ion Eu^{2+}).

Aluminum oxide has several phases that depend on the temperature with which they are synthesized, obtaining the phases χ, δ, η, γ and α; the latter is observed when the synthesis is about 1100°C. The Raman spectra that are described in [41] were measured in samples synthesized at different temperatures, indicating that when the temperature increases several of the bands disappear; this is because the $A1^{3+}$ ions change gradually from a tetrahedral structure to an octahedral coordinate structure and AlO_6 is less active for Raman; due to this is that in the α-Al_3O_3 phase there is an octahedral coordination with greater crystallinity. Previous studies on aluminum oxide have shown that the vibrational frequencies of Al-O have established that there are isolated and condensed groups of the groups AlO_4 tetrahedral and AlO_6 octahedral; being the coordination number of the cation an important parameter to determine the vibrational frequencies of Al-O. In the Fig. 7 shown the spectrum Raman for (La-Al)$_3O_3$:Eu^{2+}(5at.%)/Li+(4.5 at. %) phosphors: the band at 373 cm^{-1}, may be due to bending vibrations of AlO4 group; the band at 560 cm^{-1} may be due to condensed AlO_6; the weak bands at 635 cm^{-1} and 690 cm^{-1} may be due to isolated A104 and condensed A106 groups; the strong band at 774 cm^{-1} reveals the growth of condensed $A10_4$; because these powders were synthesized at 1250°C, only some of the bands indicated are observed [41]; that is why these bands indicate that there is a greater crystallinity in the (La-Al)$_3O_3$:Eu^{2+}(5at.%)/Li^{+}(4.5 at. %) phosphors.

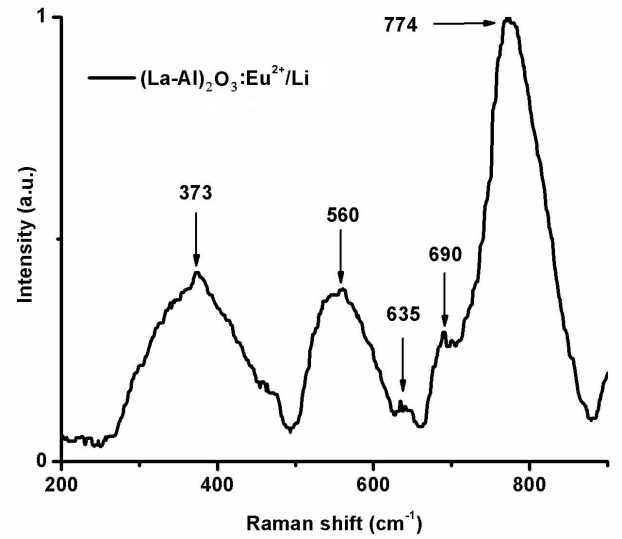

FIGURE 7. Raman spectrum of $(La\text{-}Al)_2O_3$:Eu $^{2+}$(5at.%)/Li^{+} (4.5 at. %) phosphors.

3.1. PMMA films

As mentioned above, the Eu^{2+} doped phosphors with the highest light emission intensity were incorporated into PMMA composite films deposited by drop-casting technique. Figure 8A shows the IR absorbance spectra for polymeric films, the spectra show, basically, the same bands reported for infrared spectra of PMMA [42,43], between 403 and 993 cm^{-1} and mainly at 754 cm^{-1} appears the characteristic α-methyl group vibrations, it can be seen that there is a distinct absorption band from 1148-1275 cm^{-1}, which can be attributed to the C-O-C and -OCH3 stretching vibration. The band at 1481 and 2930-2990 cm^{-1} can be attributed to the bending vibration of the C-H bonds of -CH3 group. The bands at 2930-2990 cm^{-1} can be assigned to the C-H bond stretching vibrations of the -CH3 and -CH2- groups. The band at 1665-1734 cm^{-1} shows the presence of the acrylate carboxyl group. Furthermore, there are weak absorption bands at 3440-3613 cm^{-1}, which can be attributed to the -OH group stretching and bending vibrations, respectively. No specific features related to the phosphor particles embedded in the PMMA and/or the TOPO ligands were observed, perhaps because the strong signals from the PMMA shadows them.

The Fig. 8B shows the UV-Vis-near IR characteristics of PMMA films. From this plot it is observed that non-doped films, are highly transparent (close to 99% T) in the whole visible range, and comparable to the best quality bulk PMMA [42,43]. While doped films with Eu^{2+} phosphors are absorbing at UV wavelength values (between 0 and 40 %T from 200 to 400 nm) and semi-transparent in the whole visible range (between 40 and 70 %T from 400 to 700 nm), these films have a slight white haze due to the phosphors incorporated. The transparency of these films is low but it could be improved using other deposition techniques such as spin coating [20] which could make them attractive to be used in short-wavelength optoelectronic devices, such as luminescent materials, transparent light emitters, thin-film gas sensors, and solar cell enhancers. As it was mentioned above, PMMA films were deposited by drop-casting technique, varying the solution quantity used for each film from 1 to 1.4 ml of solution, the film thickness depended directly from the solution quantity used per film, also the transparency could be affected by the film thickness, which was found to be between 6 and 12 μm. The film thickness was measured by profilometry.

The PMMA polymeric films without Eu^{2+} doped phosphors embedded did not present any luminescent emission, as expected. When the phosphors above described were embedded into the PMMA films, they kept their luminescent properties. Figure 9a shows both excitation and emission luminescent spectra for the PMMA films with the $(La\text{-}Al)_3O_3$:Eu^{2+}(5at.%)/Li^{+}(4.5 at. %) phosphors embedded. The excitation spectrum present the same two peaks at 273 and 305 nm which appear on the phosphors spectra and that correspond to the allowed transitions $4F_7$ ($^8S_{2/7}$)-$4f^6$5d of the ion Eu^{2+} [31], but in this case the 273 nm peak is higher than the 305 nm peak, it is clear that this difference is associated with the fact that the phosphors are immersed in PMMA films and perhaps this favors the 273 nm excitation mecha-

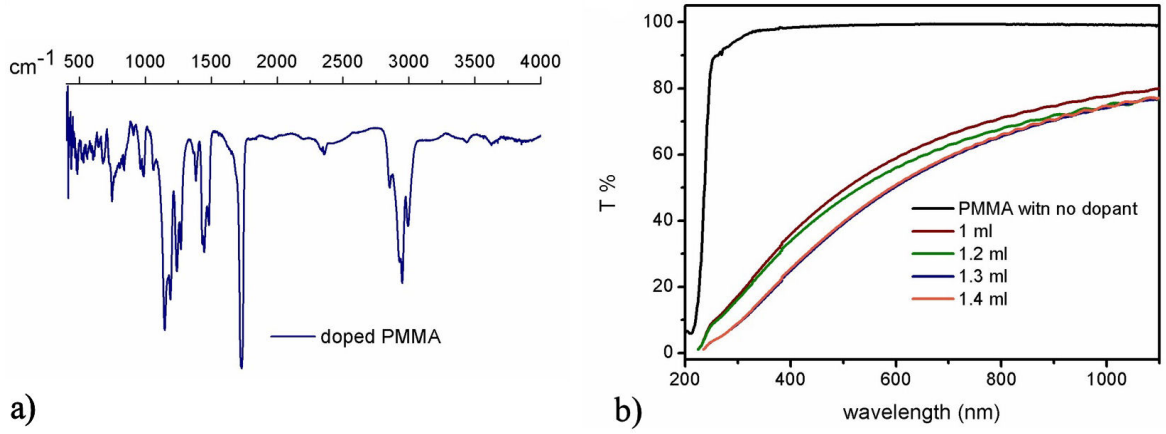

FIGURE 8. IR spectroscopy (8a) and UV-Vis transmittance (8b) measurements of PMMA films.

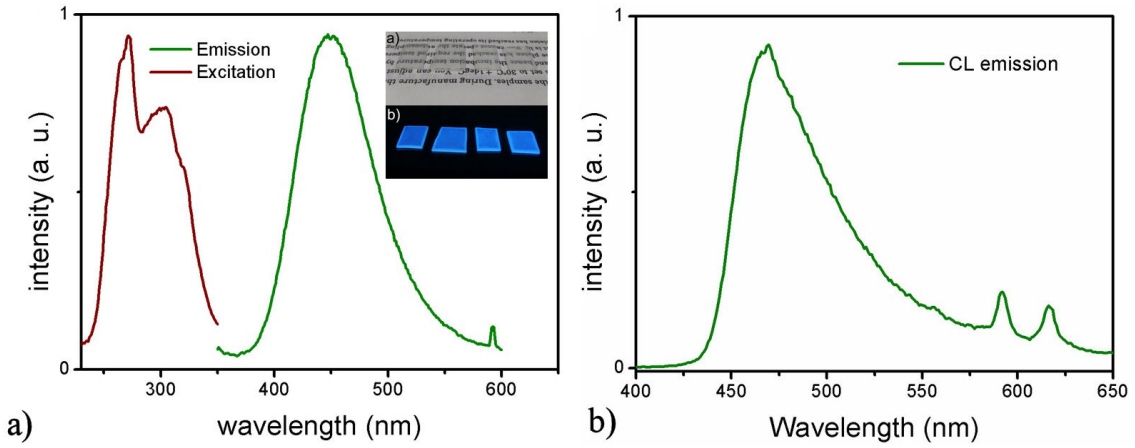

FIGURE 9. luminescent properties of PMMA films, Photoluminescence (9a) and Cathode-luminescence (9b).

nism. On the other hand, the emission spectrum, using 273 nm as excitation wavelength, has the characteristic broad blue emission peak centered at 444 nm associated with the electric-dipole allowed $4f^6 5d^1 (^8S_{7/2})$ to $4f^7$ transition, of the Eu^{2+} ion [32]. There is also, a small peak at 595 nm related to the transitions $^5D_0$ to $^7F_1$ from Eu^{3+} ion. The inset of Fig. 9a shows the transparency of films (a) and their luminescence emissions (b). The cathode-luminescence spectrum for Eu^{2+} doped PMMA films shows also the same emission characteristics as the phosphors, as can be observed in Fig 9b.

4. Conclusions

An enhancement of 320% of the Eu^{2+} broad band luminescence emission centered at 444nm was observed with the incorporation of Li^+(4.5 at. %) as co-dopant in (La-Al)$_2O_3$, (La-Al)$_2O_3$:Eu^{2+}(5at.%) phosphors, for a measured quantum efficiency of 67% when excited with 297 nm light. These phosphors were synthesized by a simple evaporation method and doped through a solid state reaction at 1250°C in a reductive atmosphere The incorporation of Eu and Eu/Li propitiate the formation of crystallites associated with the $La_{(0.827)}Al_{(11.9)}O_{(19.09)}$ and $LaAlO_3$ perovskite phases with crystallite sizes of 1 nm and 11 nm respectively. The luminescent properties of the phosphors are preserved when introduced into PMMA films. Non-doped PMMA films high transparent (99 %T) while doped films are opaque in UV region and semitransparent in the whole visible and IR ranges. The PMMA films have thicknesses between 6 and 12 μm. The spectrum Raman for (La-Al)$_2O_3$:Eu^{2+}(5at.%)/Li^+(4.5 at. %) phosphors, are present the bands at 373 cm^{-1}, 560 cm^{-1}, 635 cm^{-1}, 690 cm^{-1} and 774 cm^{-1} indicated that there is a greater crystallinity in the phosphors, because the α-Al_2O_3 phase there is an octahedral coordination, for these powders were synthesized at 1250°C.

1. Xia Shen, Ding-Fei Zhang, Xiao-Wei Fan, Guang-Shan Hu, Xian-Bin Bian and Liu Yang, *J. Mater Sci: Mater Electron* **27** (2016) 976.
2. W. A. Thornton, *J. Opt. Soc. Am.* **61** (1971) 1155.
3. L. Mariscal *et al*., *Optical Materials* **46** (2015) 233-239.
4. L. Mariscal *et al*., *ECS Journal of Solid State Science and Technology* **4,7** (2015) R97-R104.
5. L. Mariscal *et al*., *Rev. Mex. Fis.* **62** (2016) 285-289 .
6. Xue Chen, Fengzhu Lv, Yong Ma, and Yihe Zhang, *Journal of Alloys and Compounds* **680** (2016) 20-25.
7. M. Derbel *et al*., *Journal of Luminescence* **176** (2016) 356-362.
8. Zhang Lan, Li Chengyu, Su Qiang, *Journal of rare earths, Spec.* **24** (2006) 196-198.
9. L. Marciniak *et al*., *Journal of Luminescence* **170** (2016) 614-618.
10. L.K.S. de Herval *et al*., *Journal of Luminescence* **163** (2015) 17-20.
11. Syue-Liang Lin *et al*., *Journal of Luminescence* **175** (2016) 165-175.
12. S. Babu, P. Rajput, and Y. C. Ratnakaram, *J. Mater Sci* **51** (2016) 8037-8054.
13. V. Uma, K. Maheshvaran, K. Marimuthu and G. Muralidharan, *Journal of Luminescence* **176** (2016) 15-24.
14. A.I. Ramos-Guerra, J. Guzmán-Mendoza, M. García-Hipólito, O. Alvarez-Fregoso and C. Falcony, *Ceramics International* **41** (2015) 11279-11286.
15. K. Ravindranadh, R.V.S.S.N. Ravikumar and M.C. Rao, *AIP Conference Proceedings* **1728** (2016) 020079.
16. Yan-juan Li, Ming-wen Wang, Lu-dan Zhang, Duo Gao, and Shi-xiang Liu, *International Journal of Minerals, Metallurgy and Materials* **20,10** (2013) 972.
17. Hung-Rung Shih, Mu-Tsun Tsai, Lay-Gaik Teoh and Yee-Shin Chang, *Ceramics International* **41** (2015) 10595-10599.

18. Le Tien Ha, Nguyen Duc Trung Kien, Phan Huy Hoang, Thanh Tung Duong and Pham Thanh Huy, *Journal of Electronic Materials* **45** (2016) 7.
19. Zhang Xiaoting, Tomokatsu Hayakawa, Yukari Ishikawa, Yang Liushuan and Masayuki Nogami, *Journal of Alloys and Compounds* **644** (2015) 77-81.
20. E. F. Huerta, S. Carmona-Téllez, S. Gallardo-Hernández, J. G. Cabañas-Moreno and C. Falcony, *ECS Journal of Solid State Science and Technology* **5** (2016) 129-135.
21. A.N.Meza-Rocha *et al*., *Journal of Luminescence* **167** (2015) 352-359.
22. M. García-Hipólito *et al*., *Optical Materials* **22** (2003) 345-351.
23. M. J. Capitán *et al*., *J. Phys. Chem.* **99** (1995) 4655-4660.
24. M.F. Sunding *et al*., *Journal of Electron Spectroscopy and Related Phenomena* **184** (2011) 399-409.
25. E. Beyreuther, S. Grafström, L.M. Eng, Ch. Thiele and K. Dörr, *Physical Review B* **73** (2006) 155425.
26. L. Dahéron *et al*., *Chem. Mater.* **20** (2008) 583-590.
27. Kiyoshi Kanamura, Hiroshi Tamura, Soshi Shiraishi, and Zen-ichiro Takehara, *J. Electrochem. Soc.* **142** (1995) 2.
28. R. Dedryvère *et al*., *J. Phys. Chem. B* **109** (2005) 15868-15875.
29. P. Maślankiewicz, J. Szade, A. Winiarski, and Ph. Daniel, *Cryst. Res. Technol.* **40** (2005) 410-418.
30. A.T. Appapillai, A.N. Mansour, J. Cho and Y. Shao-Horn, *Chem. Mater.* **19** (2007) 5748-5757.
31. Donghyeon Kim, Jaeseong Jang, Sung Il Ahn, Sung-Hoon Kim and Jung-Chul Park, *J. Mater. Chem. C* **2** (2014) 2799-2805.
32. Sook Hyun Kwon, Byung Kee Moon, Byung Chun Choi and Jung Hyun Jeong, *Journal of the Korean Physical Society* **68** (2016) 363-367.
33. Feng Gu, Shu Fen Wang, Meng Kai Lu, Guang Jun Zhou, Dong Xu, and Duo Rong Yuan, *Langmuir* **20** (2004) 3528-3531.
34. Lingdong Sun, Cheng Qian, Chunsheng Liao, Xiaoli Wangand Chunhua Yan, *Solid State Communications* **119** (2001) 393-396.
35. Kazuo Inoue, Naoto Hirosaki, Rong-Jun Xie, and Takashi Takeda, *J. Phys. Chem. C* **113** (2009) 9392-9397.
36. Yu-Ho Won, Ho Seong Jang, Won Bin Im, Duk Young Jeon, and Jeong Soo Lee, *Applied Physics Letters* **89** (2006) 231909.
37. Yanlin Huanga and Hyo Jin Seo, *Journal of The Electrochemical Society* **158** (2011) J260-J263.
38. Zhi-yong Mao, Ying-chun Zhu, Qin-ni Fei, Da-jian Wang, *Journal of Luminescence* **131** (2011) 1048-1051.
39. R. F. Sosa, E. R. Alvarez, M. A. Camacho, A. F. Muñoz and J. 0. Rubio, *I. Phys.: Condens. Maner* **7** (1995) 65614567.
40. Kee-Sun Sohn, Sangjun Lee, Rong-Jun Xie, and Naoto Hirosaki, *Applied Physics Letters* **95** (2009) 121903.
41. P. V. Thomas, V. Ramakrishnan and V. K. Vaidyan, *Thin Solid Films* **170** (1989) 35-40.
42. S. Ramesh, Koay Hang Leen, K. Kumutha, and A. K. Arof, *Spectrochimica Acta Part A* **66** (2007) 1237.
43. Guorong Duan, Chunxiang Zhang, Aimei Li, Xujie Yan, Lude Lu, and Xin Wang, *Nanoscale Res Lett* **3** (2008) 118.